Published OnlineFirst October 13, 2014; DOI: 10.1158/2159-8290.CD-14-0621

RESEARCH BRIEF

Real-Time Intravital Imaging Establishes Tumor-Associated Macrophages as the Extraskeletal Target of Bisphosphonate Action in Cancer

Simon Junankar[1], Gemma Shay[2], Julie Jurczyluk[1], Naveid Ali[1], Jenny Down[1], Nicholas Pocock[1,3], Andrew Parker[4], Akira Nguyen[1], Shuting Sun[5], Boris Kashemirov[5], Charles E. McKenna[5], Peter I. Croucher[1], Alexander Swarbrick[1], Katherine Weilbaecher[6], Tri Giang Phan[1], and Michael J. Rogers[1]

ABSTRACT Recent clinical trials have shown that bisphosphonate drugs improve breast cancer patient survival independent of their antiresorptive effects on the skeleton. However, because bisphosphonates bind rapidly to bone mineral, the exact mechanisms of their antitumor action, particularly on cells outside of bone, remain unknown. Here, we used real-time intravital two-photon microscopy to show extensive leakage of fluorescent bisphosphonate from the vasculature in 4T1 mouse mammary tumors, where it initially binds to areas of small, granular microcalcifications that are engulfed by tumor-associated macrophages (TAM), but not tumor cells. Importantly, we also observed uptake of radiolabeled bisphosphonate in the primary breast tumor of a patient and showed the resected tumor to be infiltrated with TAMs and to contain similar granular microcalcifications. These data represent the first compelling *in vivo* evidence that bisphosphonates can target cells in tumors outside the skeleton and that their antitumor activity is likely to be mediated via TAMs.

SIGNIFICANCE: Bisphosphonates are assumed to act solely in bone. However, mouse models and clinical trials show that they have surprising antitumor effects outside bone. We provide unequivocal evidence that bisphosphonates target TAMs, but not tumor cells, to exert their extraskeletal effects, offering a rationale for use in patients with early disease. *Cancer Discov; 5(1); 35–42. ©2014 AACR.*

See related commentary by Sterling, p. 14.

INTRODUCTION

For more than two decades, bisphosphonate (BP) drugs have been the first-line therapy for the treatment and prevention of skeletal-related events in cancer patients with multiple myeloma and bone metastases, because they rapidly target the skeleton and inhibit osteoclastic bone resorption. In osteoclasts, nitrogen-containing BPs (N-BP), such as zoledronic acid (ZOL), act intracellularly by inhibiting farnesyl diphosphate (FPP) synthase, a key enzyme in the mevalonate pathway. This prevents the biosynthesis of isoprenoids necessary for the prenylation, and hence membrane localization and function, of small GTPases essential for osteoclastic bone resorption (1). Because of their high affinity for bone, the bioavailability of BPs in soft tissues is assumed to be very low. However, in various preclinical models, N-BPs have been shown to exert striking osteoclast-independent antitumor effects, including on tumors located outside the skeleton (2). Indeed, several large clinical trials in patients with breast cancer and multiple myeloma have also indicated recently that

[1]Garvan Institute of Medical Research and St. Vincent's Clinical School, Faculty of Medicine, UNSW Australia, Sydney, Australia. [2]Division of Applied Medicine, University of Aberdeen, Aberdeen, United Kingdom. [3]Department of Nuclear Medicine, St. Vincent's Hospital, Sydney, Australia. [4]Department of Pathology, St. Vincent's Hospital, Sydney, Australia. [5]University of Southern California, Los Angeles, California. [6]Department of Medicine, Washington University School of Medicine, St. Louis, Missouri.

Note: Supplementary data for this article are available at Cancer Discovery Online (http://cancerdiscovery.aacrjournals.org/).

T.G. Phan and M.J. Rogers contributed equally to this article.

Current address for G. Shay: H. Lee Moffitt Cancer Center, Tampa, Florida.

Corresponding Author: Michael J. Rogers, Garvan Institute of Medical Research, 384 Victoria Street, Darlinghurst, Sydney, NSW 2010, Australia. Phone: 61-2-9295-8273; Fax: 61-2-9295-8241; E-mail: m.rogers@garvan.org.au

doi: 10.1158/2159-8290.CD-14-0621

Published OnlineFirst October 13, 2014; DOI: 10.1158/2159-8290.CD-14-0621

N-BPs have benefits beyond inhibiting bone resorption (3). Zometa (ZOL) significantly increased disease-free survival when used alongside adjuvant endocrine therapies in women with early breast cancer (4) and in postmenopausal patients with breast cancer when used as adjuvant therapy with aromatase inhibitors or other endocrine therapies (5, 6). Importantly, ZOL also decreased the locoregional recurrence of tumors outside the skeleton (5). These findings are supported by several meta-analyses indicating significant benefits in disease-free and overall survival as well as decreased local and distant tumor recurrence. Moreover, epidemiologic studies also suggest that long-term BP therapy decreases the risk of invasive breast cancer (7). Nevertheless, there is ongoing controversy over whether N-BPs exert direct or indirect antitumor effects *in vivo*, and the cellular targets and mechanisms involved, particularly in cells outside the skeleton, have yet to be elucidated. Furthermore, ^{99m}technetium-labeled methylenebisphosphonate (^{99m}Tc-MDP, a radionuclide bone scanning agent commonly used to detect bone metastases) is recognized to accumulate in some extraskeletal tumors, including neuroblastomas, sarcomas, and breast carcinomas, although its exact mechanism of uptake in soft-tissue tumors is unclear (8). MDP is the simplest chemical form of BP and, like N-BPs, binds avidly to calcium ions and is internalized into cells by endocytosis. Therefore, to determine how BPs localize to soft-tissue tumors to exert their antitumor activity, we used intravital two-photon microscopy, together with flow cytometric analysis, to determine the cell types capable of internalizing a fluorescently labeled N-BP in a soft-tissue tumor model. We used the syngeneic 4T1 mouse model of breast cancer because treatment with ZOL has previously been shown to reduce visceral metastases in this model (9). Finally, to confirm our findings, we analyzed the uptake of ^{99m}Tc-MDP by the primary breast tumor in the preoperative bone scan of a patient and examined the postoperative resected tumor for microcalcifications and infiltration by tumor-associated macrophages (TAM).

RESULTS

N-BP Accumulates in Mammary Tumor Tissue via Leaky Tumor Vasculature

To identify the cell types capable of internalizing N-BP in tumors outside the skeleton and the route of cellular uptake, we fluorescently conjugated the N-BP risedronate to form a bone-seeking but pharmacologically inactive analogue (AF647-RIS; ref. 10) and examined its localization in mice bearing syngeneic 4T1 mammary tumors. Infrared imaging of tumor explants 24 hours after subcutaneous injection showed that AF647-RIS was detectable in whole 4T1 mammary tumors (Supplementary Fig. S1A) where it localized to the tumor periphery (Supplementary Fig. S1B). Two-photon imaging of tumor explants revealed that AF647-RIS was present intracellularly in cells located in and beneath the tumor capsule (Supplementary Fig. S1C), a region enriched for F4/80$^+$ TAMs (Supplementary Fig. S1D and S1E).

On the basis of these observations, we next examined the dynamic distribution and cellular uptake of AF647-RIS in real-time in 4T1 mammary tumors of live mice using intravital two-photon microscopy. Before imaging, TAMs were labeled *in vivo* with anti-F4/80 mAb conjugated to FITC. Imaging of second-harmonic generation by collagen fibers revealed that tumors were supplied by a dense, subcapsular network of tortuous capillaries and small blood vessels closely associated with F4/80$^+$ TAMs (Fig. 1A; Supplementary Movie S1). Immediately following intravenous injection, AF647-RIS could be visualized flowing into the vascular bed of the mammary tumors and leaking into the surrounding tumor tissue. In contrast, intravital imaging of the normal mammary fat pad of mice that did not receive 4T1 tumor cells showed rapid transit of AF647-RIS through the blood vessels in less than 5 minutes and absence of any capillary leak into mammary tissue (Fig. 1A and B; Supplementary Movie S2). The same findings were obtained using the fluorescently labeled N-BP

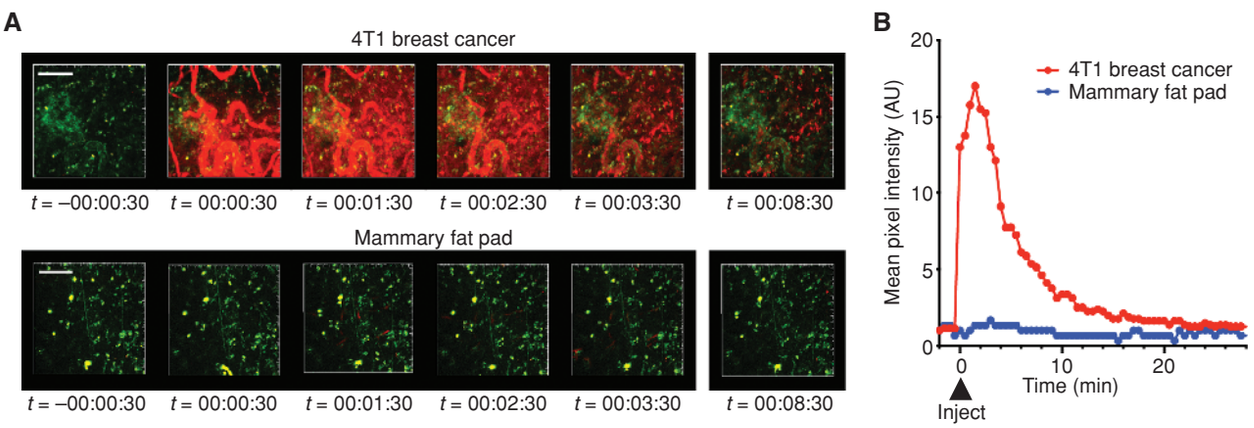

Figure 1. Dynamic *in vivo* distribution and cellular uptake of AF647-RIS in 4T1 mammary tumors. **A,** time-lapse 72-μm maximal intensity projections from the tissue surface of 4T1 breast tumor (top) and normal mammary fat pad (bottom), imaged by intravital two-photon microscopy (red, AF647-RIS; green, F4/80; the second harmonic generation signal from subcapsular collagen has been removed for clarity). Images correspond to Supplementary Movies S1 and S2. **B,** quantification of tissue distribution of AF647-RIS from **A.** Time stamp indicates hh:mm:ss after injection of AF647-RIS. Scale bar, 100 μm. Data are representative of three independent experiments.

Published OnlineFirst October 13, 2014; DOI: 10.1158/2159-8290.CD-14-0621

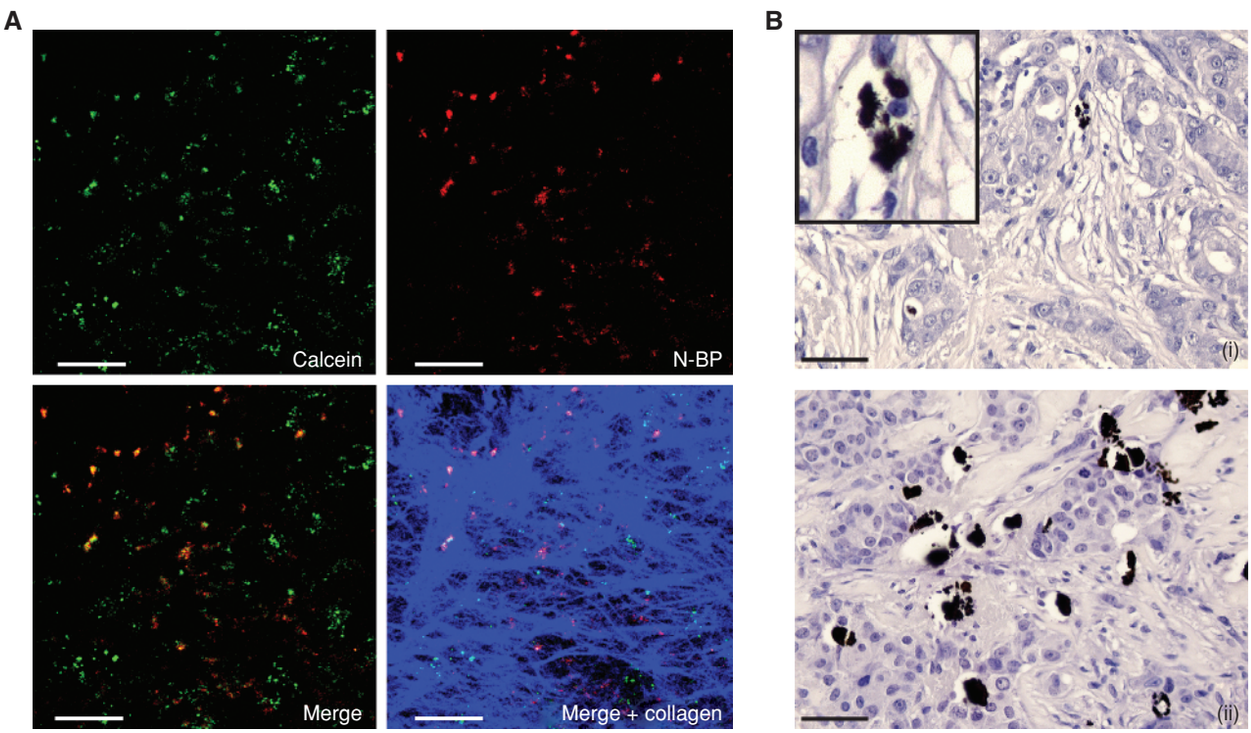

Figure 2. Detection of microcalcifications in 4T1 mammary tumors and human breast tumor tissue. **A,** two-photon imaging of whole 4T1 tumor explants 16 hours after injection of mice with calcein and N-BP shows the presence of microcalcifications labeled *in vivo* with calcein (green) or OsteoSense 680 (red), or both (yellow in the merged image). Collagen in the tumor capsule is shown in blue. **B,** von Kossa staining detects small, granular microcalcifications in sections of tumor from two different patients, (i) and (ii), with triple-negative disease (inset, a magnified region from the same section). Scale bars, 50 μm.

pamidronate (OsteoSense 680). Thus, contrary to dogma, BPs are able to access extraskeletal tumors because of the well-documented leaky new blood vessels that form in tumors (11).

TAMs Phagocytose N-BP–Coated Microcalcifications

Unbound AF647-RIS persisted in 4T1 tumor blood vessels and mammary tumor tissue for more than 15 minutes after injection of mice (Fig. 1A and B) and was observed to rapidly (within minutes) bind 2- to 5-μm granular clumps. These microstructures were calcified, because they bound the calcium-seeking dye calcein *in vivo* as well as N-BP (Fig. 2A). Image analysis of a 425 × 425 × 150 μm volume (i.e., 51 optical sections) of tumor showed that 43% of N-BP colocalized with calcein, with a Pearson correlation of 0.4 (Supplementary Fig. S2). These structures closely resembled the small granules of microcalcification (distinct from the larger calcifications present in the lumen of mammary ducts) that we detected histologically in sections of random human breast cancer tissue by von Kossa staining (Fig. 2Bi and ii). In an additional 40 samples of human breast tumor tissue, 40% showed evidence of these small, granular microcalcifications (3/10 ER^+ tumors, 4/10 ER^+Her2^+ tumors, 2/10 ER^-Her2^+ tumors, and 7/10 triple-negative tumors).

Importantly, in mice with 4T1 mammary tumors, $F4/80^+$ TAMs were observed to bind and internalize small, subcellular complexes of AF647-RIS by pinocytosis (Fig. 3A; Supplementary Movie S3), whereas AF647-RIS bound to microcalcified granules was engulfed by phagocytosis (Fig. 3B; Supplementary Movie S4). Notably, we did not observe any uptake in any non–F4/80-labeled cells such as epithelial cells. Imaging of mice 24 hours following AF647-RIS administration indicated that the bulk of the AF647-RIS was localized in the cytoplasm of $F4/80^+$ cells, confirming the uptake by TAMs (Fig. 3C; Supplementary Movie S5).

We also examined the uptake of fluorescently labeled N-BP in mice bearing subcutaneous B16.F10 melanomas. Although we also observed some leakage of N-BP from tumor capillaries, in contrast with 4T1 tumors, we did not observe any binding to granular calcifications or retention of N-BP in the tumor tissue (Supplementary Fig. S3A). Although we did detect some calcein staining in the B16 tumors, this was considerably less than in the 4T1 tumors (Supplementary Fig. S3B). Consistent with this, FACS analysis showed little uptake of N-BP by TAMs in B16 tumors (Supplementary Fig. S3C). This suggests that the presence of microcalcifications in tumors strongly enhances the efficiency of uptake of N-BP by TAMs.

N-BP Is Efficiently Internalized *In Vivo* by TAMs but Not by Tumor Cells

To confirm the phenotype of the cells responsible for uptake of N-BP, we performed multiparameter flow cytometric analysis of enzymatically digested, single-cell suspensions

Published OnlineFirst October 13, 2014; DOI: 10.1158/2159-8290.CD-14-0621

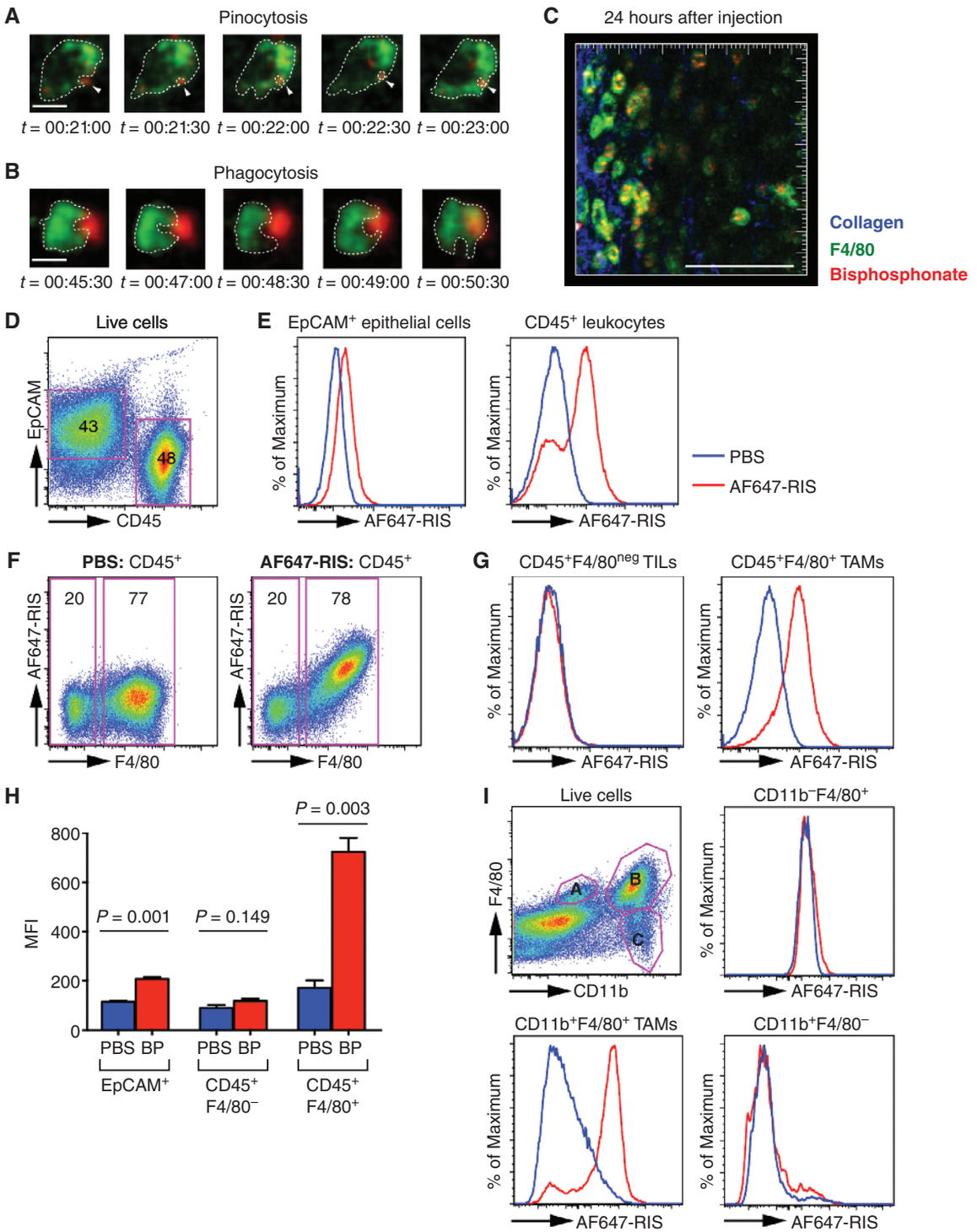

Figure 3. AF647-RIS is internalized by TAMs *in vivo*. **A** and **B,** time-lapse images from a single optical plane showing uptake of small (**A**) and large (**B**) AF647-RIS complexes (red) by F4/80-labeled macrophages (green); images correspond to Supplementary Movies S3 and S4 and are representative of three independent experiments, with at least three single cells analyzed per experiment. **C,** 60-μm maximal intensity projection from the surface of 4T1 breast tumor 24 hours after injection of AF647-RIS. Blue, collagen; green, F4/80; red, AF647-RIS. Images correspond to Supplementary Movie S5. Scale bars, 10 μm in **A** and **B**, and 100 μm in **C**. Time stamp, hh:mm:ss after injection of AF647-RIS. **D,** FACS staining of mammary epithelial cells for EpCAM and tumor-infiltrating leukocytes (TIL) for CD45. **E,** histogram, AF647-RIS signal in mammary epithelial cells and TILs in mice treated with PBS (blue) or AF647-RIS (red). **F,** the pseudocolor plot showing AF647-RIS and F4/80 gated on CD45+ cells in mice treated with PBS (left) or AF647-RIS (right). **G,** histogram, AF647-RIS signal in $CD45^+F4/80^-$ TILs and $CD45^+F4/80^+$ TAMs in mice treated with PBS (blue) or AF647-RIS (red). **H,** quantification of AF647-RIS (BP) uptake. MFI, mean fluorescence intensity. **I,** FACS analysis of AF647-RIS (red) or PBS (blue) uptake by subpopulations of F4/80+ TAMs. Data are the mean ± SEM and are representative of at least two independent experiments with $n = 3$ mice in each group.

Published OnlineFirst October 13, 2014; DOI: 10.1158/2159-8290.CD-14-0621

of tumors. 4T1 tumors consisted of a large infiltrate of immune cells, with about 50% of the cells being CD45$^+$ tumor-infiltrating leukocytes (TIL; Fig. 3D). There was minor uptake of AF647-RIS by EpCAM$^+$ mammary epithelial cells (Fig. 3E), with a small shift in mean fluorescence intensity (MFI) that was below the limit of detection of our intravital imaging modalities (Fig. 1A and B). The bulk of AF647-RIS, however, was taken up by a major subpopulation of CD45$^+$ leukocytes (Fig. 3E). Analysis for F4/80 expression confirmed that these cells were F4/80$^+$ TAMs (Fig. 3F and G), confirming the results of the intravital imaging studies (Fig. 3C; Supplementary Movie S5). Significantly, quantification of the MFI showed a near 5-fold increase in AF647-RIS MFI in CD45$^+$ F4/80$^+$ TAMs compared with a <2-fold increase in tumor epithelial cells and no increase in CD45$^+$ F4/80^{neg} TILs (Fig. 3G and H). Further analysis showed that the F4/80$^+$ TAMs that internalized AF647-RIS were also CD11b$^+$ (Fig. 3I). Collectively, these data identify TAMs as the cell type targeted by N-BP in mammary tumors.

Clinicopathologic Correlation of Bisphosphonate Uptake in Human Breast Cancer with Microcalcifications and TAMs

A 51-year-old female patient presented with a grade 1 invasive duct carcinoma associated with ductal carcinoma *in situ* and focal lymphovascular invasion (whole tumor size, 16 mm). A routine bone scintigraphy scan using ^{99m}Tc-MDP and multimodal single-photon emission computed tomography (SPECT)/CT imaging revealed clear uptake of the radionuclide in the mammary carcinoma (Fig. 4A). Sections of the resected tumor of this patient showed extensive CD68$^+$ and CD163$^+$ macrophage infiltration (Fig. 4Bi and ii). Furthermore, von Kossa staining revealed the presence of small, granular calcifications within the mammary tumor tissue (Fig. 4Biii) and in adjacent benign tissue (Fig. 4Biv and v) that were similar in size and appearance to those observed to bind N-BP and be internalized by TAMs in the mouse 4T1 tumors. Some of these granular microcalcifications in the human tumor tissue were also closely associated with, or even appeared to have been internalized by, CD68$^+$ or CD163$^+$ macrophages (Fig. 4Bii/iii and iv/v).

DISCUSSION

The exact mechanism underlying the *in vivo* antitumor activity of N-BPs has been highly controversial because it is not clear which cell types internalize these drugs in tumors, particularly outside the skeleton. Other studies have shown that N-BP treatment can affect the mevalonate pathway in subcutaneous or peritoneal tumors in mouse models *in vivo*, but these reports did not identify the exact cell types involved (12–14). Our data show unequivocally that, in 4T1 mammary tumors, N-BP is rapidly and efficiently internalized by TAMs rather than tumor cells. This is consistent with reports that ZOL treatment reduces the number of TAMs in mouse models of mammary and cervical cancer (15, 16). It appears that TAMs have a selective ability to internalize N-BPs that is shared with other myeloid lineage cells such as peripheral blood and bone marrow monocytes, peritoneal macrophages, and osteoclasts (17), and is most likely related to the capacity of these cells for pinocytosis and phagocytosis of calcium-containing complexes (such as microcalcifications), because there is no evidence for any other specific transport mechanisms for cellular uptake of these drugs (18). Indeed, engulfment of N-BP–coated microcalcifications may be the major route of uptake by TAMs *in vivo* because we observed little uptake of N-BP by TAMs in B16 tumors that lacked extensive binding of N-BP to microcalcifications.

Small, granular microcalcifications are common in human breast tumors because we identified their presence in 40% of the tissue samples examined. In mouse 4T1 tumors, microcalcified granules were also found to be present throughout the tumor tissue; the particular localization and retention of AF647-RIS in the tumor periphery presumably reflect the high density of leaky vessels in this region. The time course of the distribution and cellular uptake of AF647-RIS in 4T1 tumors (within 30 minutes of injection) is entirely consistent with the rapid localization of ^{99m}Tc-MDP in breast tumors observed in some patients by scintigraphic imaging (19). Our observations therefore identify the likely mechanism of soft-tissue tumor localization of ^{99m}Tc-MDP in humans by a similar mechanism to that observed in mice, that is, via leaky tumor vessels and binding to granular microcalcifications that are engulfed by TAMs. This provides a mechanistic explanation for a phenomenon that was first described 40 years ago (20) but remains poorly characterized.

In osteoclasts and macrophages, inhibition of FPP synthase by N-BPs and the subsequent loss of prenylation of small GTPases affect numerous processes, including polarization, adhesion, migration, vesicular trafficking, proliferation, and survival (1, 21). It is highly likely that N-BP treatment also affects multiple functions of TAMs *in vivo* by inhibiting protein prenylation. TAMs have emerged as powerful promoters of tumor growth and metastasis (22), and extensive macrophage infiltration in many tumor types is associated with poor patient prognosis (23). Our studies indicate that the antitumor activity of N-BPs observed in preclinical models and in clinical trials is likely mediated indirectly through uptake of these drugs by TAMs and possibly other myeloid lineage cells, leading to their functional impairment and depletion, rather than by direct effects on tumor cells *per se*. These observations provide a further rationale for the use of N-BP as adjuvant cancer therapy in patients with early-stage disease.

METHODS

SPECT/CT Imaging of Patients

Radionuclide bone scans were performed using 900MBq ^{99m}Tc-MDP (technetium-99m-methylene diphosphonate; RadPharm) followed by multimodal SPECT/CT imaging after 3 hours using a GE Discovery NM/CT 670 with BrightSpeed Elite16 slice CT and Advanced Elite NXT SPECT detectors.

Preclinical Mouse Tumor Models

Immunocompetent BALB/c mice ages 6 to 8 weeks were obtained from Australian BioResources (Moss Vale) and housed at the Garvan Institute of Medical Research; 4T1-Luc2 cells were purchased from PerkinElmer and used within 6 months without authentication. For tumor transplantation, 4T1 cells were resuspended in PBS and 5×10^5 cells in a 10-μL volume were injected into the fourth inguinal mammary fat pad. B16.F10 cells were purchased from the ATCC and used within 6 months (passage 2). Cells (2×10^6) in a 50-μL volume

Published OnlineFirst October 13, 2014; DOI: 10.1158/2159-8290.CD-14-0621

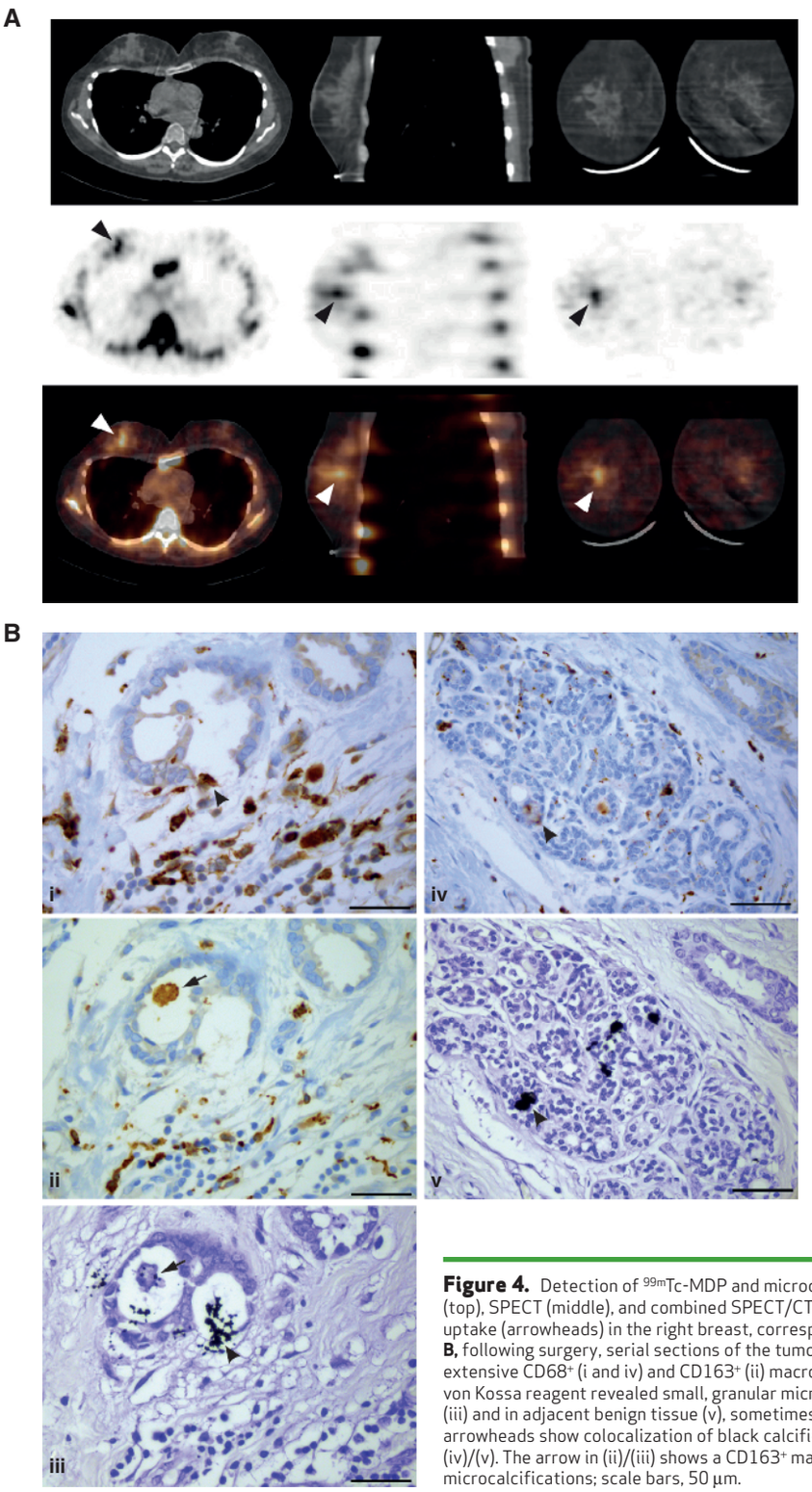

Figure 4. Detection of ^{99m}Tc-MDP and microcalcifications in human breast tumor. **A,** the CT (top), SPECT (middle), and combined SPECT/CT (bottom) images show increased ^{99m}Tc-MDP uptake (arrowheads) in the right breast, corresponding to the carcinoma visible in the CT slice. **B,** following surgery, serial sections of the tumor from the same patient showed the presence of extensive CD68$^+$ (i and iv) and CD163$^+$ (ii) macrophage infiltration. Serial sections stained with von Kossa reagent revealed small, granular microcalcifications (black) within the tumor tissue (iii) and in adjacent benign tissue (v), sometimes closely associated with CD68$^+$ macrophages; arrowheads show colocalization of black calcifications and brown CD68$^+$ staining in (i)/(iii) and (iv)/(v). The arrow in (ii)/(iii) shows a CD163$^+$ macrophage that appears to contain intracellular microcalcifications; scale bars, 50 μm.

Published OnlineFirst October 13, 2014; DOI: 10.1158/2159-8290.CD-14-0621

were inoculated subcutaneously into the flanks of C57/BL6 mice. Mice were administered a single dose of N-BP (0.9 mg/kg AF647-RIS or 0.7 mg/kg OsteoSense 680) or 70 mg/kg calcein 10 to 14 days after tumor cell inoculation.

Intravital Two-Photon Microscopy of 4T1 Mammary Tumors

We used a Zeiss 7MP two-photon microscope (Carl Zeiss) excited by a Chameleon Vision II Ti:Sa laser (Coherent Scientific) with filters and detectors as described previously (24). Intravital two-photon microscopy of mammary fat pad and 4T1 tumors was based on the method for imaging the medullary surface of inguinal lymph nodes (25). See Supplementary Methods for additional details.

Flow Cytometry

Mice with palpable mammary tumors received a single s.c. injection of N-BP (0.9 mg/kg AF647-RIS or 0.7 mg/kg OsteoSense 680). Twenty-four hours later, the mice were perfused with PBS and euthanased. Tumors were mechanically dispersed and enzymatically digested (Collagenase Blend L; Sigma) using a gentleMACS (Milltenyi Biotech) tissue dissociator, incubated with DNase (1 mg/mL; Sigma), then passed through a 70-μm nylon strainer (BD Biosciences). Erythrocytes were lysed using ammonium chloride, and the remaining cells were washed once in PBS, blocked with anti-CD16/32 (eBiosciences) for 10 minutes on ice, then stained with antibodies to CD45 (APC-AF750, from eBiosciences), F4/80 (FITC, from UCSF Hybridoma Core Facility), and EpCAM (PerCP-Cy5.5, from BioLegend), before analysis on a LSRII SORP flow cytometer using BD FACS DIVA software. Data were analyzed using FlowJo software (Treestar Inc.). For detection of AF647-RIS uptake, cells from the tumors of vehicle-treated animals were used as controls for background fluorescence. Fluorescence due to AF647-RIS uptake was measured as the geometric mean in the R670-nm channel, in $CD45^+EpCAM^-$ or $CD45^-EpCAM^+$ populations.

Histology

Ethics approval was granted for the use of pathology specimens and cognate clinicopathologic data (Human Research Ethics Committee of St. Vincent's Hospital, Sydney, NSW, Australia). For von Kossa staining of microcalcifications, 5-μm formalin-fixed, paraffin-embedded sections of tumor were dewaxed and hydrated with distilled water, and then incubated in 1% silver nitrate in bright light for 1 hour. Sections were then incubated in 5% sodium thiosulphate for 5 minutes and counterstained with 1% toluidine blue for 30 seconds. Slides were then dehydrated and cleared before mounting in Eukitt mounting medium. Serial sections were immunostained for CD163 (clone 10D6; Novocastra) or CD68 (Ventana predilute KP1 antibody) using a standard protocol on a Ventana XT machine with CC1 antigen retrieval, brown chromogen, and hematoxylin counterstain. Images were captured using a Leica DM 6000 Power Mosaic microscope with a DFC310FX camera. See Supplementary Methods for additional details of immunostaining.

Ethical Statement

Written, informed consent was obtained from the patient for the use of deidentified SPECT/CT images. Animal experiments were approved by the Garvan Institute of Medical Research/St. Vincent's Hospital Animal Experimentation Ethics Committee (AEC 12_41).

Statistical Analysis

The unpaired, two-sided Student *t* test with Welch correction was performed using Prism software (GraphPad).

Disclosure of Potential Conflicts of Interest

N. Pocock has received honoraria from the speakers' bureaus of MSD and Sanofi. S. Sun is chief operating officer and a consultant/advisory board member for BioVinc LLC. C.E. McKenna has ownership interest (including patents) and is a consultant/advisory board member for BioVinc LLC. P.I. Croucher reports receiving a commercial research grant from Novartis Pharma. M.J. Rogers reports receiving a commercial research grant from Warner Chilcott and has received honoraria from the speakers' bureaus of Novartis and MSD. No potential conflicts of interest were disclosed by the other authors.

Authors' Contributions

Conception and design: S. Junankar, G. Shay, N. Pocock, C.E. McKenna, T.G. Phan, M.J. Rogers

Development of methodology: S. Junankar, G. Shay, N. Pocock, S. Sun, A. Swarbrick, T.G. Phan, M.J. Rogers

Acquisition of data (provided animals, acquired and managed patients, provided facilities, etc.): S. Junankar, G. Shay, J. Jurczyluk, N. Ali, N. Pocock, A. Parker, A. Nguyen, A. Swarbrick, K. Weilbaecher, T.G. Phan, M.J. Rogers

Analysis and interpretation of data (e.g., statistical analysis, biostatistics, computational analysis): S. Junankar, G. Shay, A. Parker, P.I. Croucher, K. Weilbaecher, T.G. Phan, M.J. Rogers

Writing, review, and/or revision of the manuscript: S. Junankar, G. Shay, N. Pocock, A. Parker, S. Sun, C.E. McKenna, P.I. Croucher, K. Weilbaecher, T.G. Phan, M.J. Rogers

Administrative, technical, or material support (i.e., reporting or organizing data, constructing databases): J. Jurczyluk, N. Ali, J. Down, B. Kashemirov, T.G. Phan

Study supervision: T.G. Phan, M.J. Rogers

Other (designed and synthesized the probe reagents used in the study): S. Sun

Other (design, synthesis, and application of fluorescent probe): C.E. McKenna

Acknowledgments

The authors thank Dr. Hal Ebetino for his support in the development of fluorescent bisphosphonates for *in vivo* imaging; Mehreen Arshi, Mary Hornick, Natasa Kovacic, and Michelle McDonald for technical assistance; Prof. Antony Basten for comments on the article; and Tyani Chan for proofreading.

Grant Support

This work was funded by project grant RG 14-12 from the Cancer Council NSW (to M.J. Rogers and T.G. Phan). T.G. Phan was also supported by a Career Development Fellowship (APP 1005097) and Project Grant APP 1004632 from the National Health and Medical Research Council of Australia (NHMRC). The contents of this article are solely the responsibility of the administering institution, a participating institution, or individual authors and do not reflect the views of NHMRC. K. Weilbaecher was supported by RO1-CA097250. G. Shay was funded by a studentship from the Fraserburgh Moonlight Prowl, facilitated by Prof. S. Heys, University of Aberdeen. Tissues and samples were received from the Australia Breast Cancer Tissue Bank, which is generously supported by the National Health and Medical Research Council of Australia, The Cancer Institute NSW, and the National Breast Cancer Foundation.

The costs of publication of this article were defrayed in part by the payment of page charges. This article must therefore be hereby marked *advertisement* in accordance with 18 U.S.C. Section 1734 solely to indicate this fact.

Received June 16, 2014; revised October 2, 2014; accepted October 8, 2014; published OnlineFirst October 13, 2014.

REFERENCES

1. Rogers MJ, Crockett JC, Coxon FP, Monkkonen J. Biochemical and molecular mechanisms of action of bisphosphonates. Bone 2011; 49:34–41.

Published OnlineFirst October 13, 2014; DOI: 10.1158/2159-8290.CD-14-0621

2. Clezardin P. Bisphosphonates' antitumor activity: an unravelled side of a multifaceted drug class. Bone 2011;48:71–9.
3. Coleman R, Gnant M, Morgan G, Clezardin P. Effects of bone-targeted agents on cancer progression and mortality. J Natl Cancer Inst 2012;104:1059–67.
4. Gnant M, Mlineritsch B, Schippinger W, Luschin-Ebengreuth G, Postlberger S, Menzel C, et al. Endocrine therapy plus zoledronic acid in premenopausal breast cancer. N Engl J Med 2009;360:679–91.
5. Coleman RE, Marshall H, Cameron D, Dodwell D, Burkinshaw R, Keane M, et al. Breast-cancer adjuvant therapy with zoledronic acid. N Engl J Med 2011;365:1396–405.
6. Coleman R, de Boer R, Eidtmann H, Llombart A, Davidson N, Neven P, et al. Zoledronic acid (zoledronate) for postmenopausal women with early breast cancer receiving adjuvant letrozole (ZO-FAST study): final 60-month results. Ann Oncol 2013;24:398–405.
7. Chlebowski RT, Chen Z, Cauley JA, Anderson G, Rodabough RJ, McTiernan A, et al. Oral bisphosphonate use and breast cancer incidence in postmenopausal women. J Clin Oncol 2010;28:3582–90.
8. Worsley DF, Lentle BC. Uptake of technetium-99m MDP in primary amyloidosis with a review of the mechanisms of soft tissue localization of bone seeking radiopharmaceuticals. J Nucl Med 1993;34:1612–5.
9. Hiraga T, Williams PJ, Ueda A, Tamura D, Yoneda T. Zoledronic acid inhibits visceral metastases in the 4T1/luc mouse breast cancer model. Clin Cancer Res 2004;10:4559–67.
10. Roelofs AJ, Coxon FP, Ebetino FH, Lundy MW, Henneman ZJ, Nancollas GH, et al. Fluorescent risedronate analogues reveal bisphosphonate uptake by bone marrow monocytes and localization around osteocytes *in vivo*. J Bone Miner Res 2010;25:606–16.
11. McDonald DM, Baluk P. Significance of blood vessel leakiness in cancer. Cancer Res 2002;62:5381–5.
12. Guenther A, Gordon S, Tiemann M, Burger R, Bakker F, Green JR, et al. The bisphosphonate zoledronic acid has antimyeloma activity *in vivo* by inhibition of protein prenylation. Int J Cancer 2010;126:239–46.
13. Ottewell PD, Lefley DV, Cross SS, Evans CA, Coleman RE, Holen I. Sustained inhibition of tumor growth and prolonged survival following sequential administration of doxorubicin and zoledronic acid in a breast cancer model. Int J Cancer 2010;126:522–32.
14. Benzaid I, Monkkonen H, Bonnelye E, Monkkonen J, Clezardin P. *In vivo* phosphoantigen levels in bisphosphonate-treated human breast tumors trigger Vgamma9Vdelta2 T-cell antitumor cytotoxicity through ICAM-1 engagement. Clin Cancer Res 2012;18:6249–59.
15. Melani C, Sangaletti S, Barazzetta FM, Werb Z, Colombo MP. Amino-biphosphonate-mediated MMP-9 inhibition breaks the tumor-bone marrow axis responsible for myeloid-derived suppressor cell expansion and macrophage infiltration in tumor stroma. Cancer Res 2007;67:11438–46.
16. Giraudo E, Inoue M, Hanahan D. An amino-bisphosphonate targets MMP-9-expressing macrophages and angiogenesis to impair cervical carcinogenesis. J Clin Invest 2004;114:623–33.
17. Roelofs AJ, Thompson K, Ebetino FH, Rogers MJ, Coxon FP. Bisphosphonates: molecular mechanisms of action and effects on bone cells, monocytes and macrophages. Curr Pharm Des 2010;16:2950–60.
18. Thompson K, Rogers MJ, Coxon FP, Crockett JC. Cytosolic entry of bisphosphonate drugs requires acidification of vesicles after fluid-phase endocytosis. Mol Pharmacol 2006;69:1624–32.
19. Piccolo S, Lastoria S, Mainolfi C, Muto P, Bazzicalupo L, Salvatore M. Technetium-99m-methylene diphosphonate scintimammography to image primary breast cancer. J Nucl Med 1995;36:718–24.
20. Berg GR, Kalisher L, Osmond JD, Pendergrass HP, Potsaid MS. 99mTc-diphosphonate concentration in primary breast carcinoma. Radiology 1973;109:393–4.
21. Itzstein C, Coxon FP, Rogers MJ. The regulation of osteoclast function and bone resorption by small GTPases. Small GTPases 2011;2:117–30.
22. Joyce JA, Pollard JW. Microenvironmental regulation of metastasis. Nat Rev Cancer 2009;9:239–52.
23. Bingle L, Brown NJ, Lewis CE. The role of tumour-associated macrophages in tumour progression: implications for new anticancer therapies. J Pathol 2002;196:254–65.
24. Chtanova T, Hampton HR, Waterhouse LA, Wood K, Tomura M, Miwa Y, et al. Real-time interactive two-photon photoconversion of recirculating lymphocytes for discontinuous cell tracking in live adult mice. J Biophotonics 2014;7:425–33.
25. Grigorova IL, Schwab SR, Phan TG, Pham TH, Okada T, Cyster JG. Cortical sinus probing, S1P1-dependent entry and flow-based capture of egressing T cells. Nat Immunol 2009;10:58–65.

Published OnlineFirst October 13, 2014; DOI: 10.1158/2159-8290.CD-14-0621

AACR American Association for Cancer Research

CANCER DISCOVERY

Real-Time Intravital Imaging Establishes Tumor-Associated Macrophages as the Extraskeletal Target of Bisphosphonate Action in Cancer

Simon Junankar, Gemma Shay, Julie Jurczyluk, et al.

Cancer Discovery 2015;5:35-42. Published OnlineFirst October 13, 2014.